Co-published by
**Institute of Fluid-Flow Machinery**
Polish Academy of Sciences
**Committee on Thermodynamics and Combustion**
Polish Academy of Sciences



http://www.imp.gda.pl/archives-of-thermodynamics/

# Heat transfer optimization of MHD unsteady separated stagnation-point flow of a hybrid ferrofluid with heat generation

Amirul Zaqwan Azman[a], Norihan Md Arifin[a*], Nur Syahirah Wahid[a], Mohd Ezad Hafidz Hafidzuddin[b]

[a]Department of Mathematics & Statistics, Faculty of Science, Universiti Putra Malaysia, 43400, UPM Serdang, Selangor, Malaysia
[b]Centre of Foundation Studies for Agricultural Science, Universiti Putra Malaysia, 43400 UPM Serdang, Selangor
*Corresponding author email: norihana@upm.edu.my

Received: 23.12.2024; revised: 04.03.2025; accepted: 20.03.2025

## Abstract

The heat transfer optimization for magnetohydrodynamic unsteady stagnation-point flows and the thermal progress with the effect of heat generation is performed using the response surface methodology. The first step in this study involves reducing the mathematical model of partial differential equations and boundary conditions into non-linear ordinary differential equations via similarity transformations. Numerical solutions of the emerged system are obtained using the bvp4c solver. As observed from this study, the magnitude of the skin friction coefficient and heat transfer rate rises with the suction parameter. The statistical analysis and optimization done using the response surface methodology revealed that the suction parameter highly impacts the local Nusselt number. The maximum sensitivity of the heat transfer rate is towards the magnetic and suction parameters.

**Keywords:** Stagnation-point flow; Magnetohydrodynamic; Hybrid ferrofluid; Heat generation; Permeable

Vol. 46(2025), No. 2, 93–102; doi: 10.24425/ather.2025.154909

Cite this manuscript as: Azman, A.Z., Arifin, N.M., Wahid, N.S., & Hafidzuddin, M.E.H. (2025). Heat transfer optimization of MHD unsteady separated stagnation-point flow of a hybrid ferrofluid with heat generation. *Archives of Thermodynamics*, 46(2), 93–102.

## 1. Introduction

Heat transfer has been the focus of many researchers due to its wide application. One important material property that controls heat transfer efficiency is thermal conductivity, a higher conductivity allows thermal energy to move through the medium more quickly. Magnetohydrodynamics (MHD) describes the behaviour of electrically conducting fluids and has crucial applications in engineering, astrophysics and fusion energy research. For example, axisymmetric MHD Homann flow over a stretching and spiralling disk in the stagnation region was analysed by Khan et al. [1]. Many studies have found that solid-type nanoparticles with high thermal conductivity can raise the fluid thermal conductivity to intensify the heat transfer rate. Nanofluids, consisting of a blend of two distinct nanoparticles dispersed in a base liquid, are employed to boost heat transfer efficiency owing to their enhanced thermal conductivity compared to the base liquid. These fluids have shown promising results in improving energy efficiency in various applications, especially industries that require thermal management. Choi and Eastman [2] were the first to introduce the concept of nanofluids. Later, Eastman et al. [3] investigated their thermal conductivity and heat transfer properties. Since then, numerous researchers have conducted extensive theoretical studies on the thermal conductivity of nanofluids. Recently, Sarfraz et al. [4] examined Walter's B nanofluid heat and mass flow, and dual solutions were obtained. They show that the activation energy parameter enhances mass distribution in both solutions.

## Nomenclature

$B_0$ – magnetic field effect, T
$C$ – number centre points
$C_p$ – heat capacity, J/(kg·K)
$c$ – coefficients
$F$ – number of factors
$k$ – thermal conductivity, W/(m·K)
$M$ – dimensionless magnetic parameter
$N$ – number of independent variables
Nu – Nusselt number
Pr – Prandtl number
$Q_H$ – dimensionless heat generation parameter (or $Q$)
$Q_h$ – heat generation effect, W/m$^3$
$q_w$ – local Nusselt number
Re – Renolds number
$S$ – dimensionless suction parameter
$T_w$ – wall temperature, K
$T_\infty$ – farfield temperature, K
$t$ – time, s
$t_{ref}$ – constant reference time, s
$u$, $v$ – component velocity, m/s
$u_0$ – velocity of the plate, m/s
$u_e$ – free stream velocity, m/s
$v_0$ – mass suction/injection, m/s
$v_w$ – velocity of wall mass transfer, m/s
$x$, $y$ – Cartesian coordinate, m
$x_0$ – displacement of the plate, m
$x1$ – coded symbol for the magnetic parameter
$x2$ – coded symbol for the heat generation parameter
$x3$ – coded symbol for the suction parameter

### Greek symbols

$\alpha$ – strength of free stream velocity
$\beta$ – unsteadiness parameter
$\mu$ – dynamic viscosity, kg/(m·s)
$\nu$ – kinematic viscosity, m$^2$/s
$\rho$ – density, kg/m$^3$
$\sigma$ – electrical conductivity, S/m
$\tau$ – local skin friction coefficient
$\phi$ – nanoparticles volume fraction

### Subscripts and Superscripts

$f$ – base fluid
$hnf$ – hybrid nanofluid
$nf$ – mono nanofluid

### Abbreviations and Acronyms

ANOVA – analysis of variance
DOE – design of experiment
MHD – magnetohydrodynamics
RSM – response surface methodology
USSP – unsteady separated stagnation point (flow)

Ferrofluid is a stable colloidal mixture where ferromagnetic particles are suspended in a liquid, using standard base fluids such as water, oil and similar liquids. The composition of a ferrofluid includes three key components; magnetic nanoparticles, a dispersion medium (the carrier liquid) and a dispersant. Hybrid ferrofluid is a unique heat transfer fluid because it can be controlled magnetically and is ideal for wide applications. Several researchers have investigated the efficiency of hybrid ferrofluid as a heat transfer fluid. The stagnation-point flow on exponentially stretching/shrinking surfaces for hybrid ferrofluids with magnetic effect was examined by Anuar et al. [5], and significant improvement was found in utilizing hybrid ferrofluids. The unsteady hybrid ferrofluid flow over a cylinder examined by Saranya et al. [6] also considerably benefits from the viscous–ohmic dissipative effect. To evaluate the impact of the unsteadiness parameter on the thermal rate, Waini et al. [7] studied the unsteady MHD flow of hybrid ferrofluid over a rotating disk. Another numerical study on the effects of MHD and heat generation for the time-dependent separated stagnation-point flow of hybrid ferrofluid on a moving plate was carried out by Khashi'ie et al. [8]. Many other works reported in this field [9–11].

The influence of heat generation or absorption plays a crucial role in altering the temperature distribution in various applications, particularly those involving dissociating fluids and chemical reactions. The study of unsteady stagnation-point flow in hybrid nanofluids has gained significant interest due to its applications in industries such as cooling systems, chemical processes and thermal management technologies. Hybrid nanofluids, which combine two or more types of nanoparticles in a base fluid, exhibit superior thermal and flow properties compared to conventional fluids or mono-nanofluids. Unsteady stagnation-point flow describes the time-dependent interaction of fluid meeting a surface perpendicularly before diverging tangentially. The introduction of hybrid nanofluids to this flow system has been studied extensively for its ability to enhance heat transfer and fluid dynamics. Zainal et al. [12] investigated the thermophysical properties of the unsteady separated stagnation-point flow past a moving plate by a hybrid nanofluid. Khan et al. [13] concluded that the combination of $Al_2O_3$ and Cu nanoparticles in hybrid nanofluids improves thermal conductivity and increases the heat transfer rate. Their research shows that the heat generation parameter further enhances temperature profiles, while heat absorption mitigates thermal effects. The unsteadiness parameter, representing time-dependent changes in flow behaviour, significantly affects velocity and temperature profiles. Mahmood and Khan [14] found that decreasing unsteadiness enhances heat transfer but increases flow resistance. Additional studies of flow via the boundary layer and heat transfer are available in [15–19].

A variety of studies have investigated heat sources or sinks that depend on temperature across different geometrical configurations. Hybrid nanofluid slip flow over an exponentially stretching/shrinking permeable sheet with heat generation was analysed by Wahid et al. [20]. Consequently, the thermal boundary layer thickness is observed to expand with heat generation and contract with heat absorption. Further analyses on the effects of heat generation were discussed in [21,22]. Furthermore, Yasir and Khan [23] studied the impact of internal heat generation on thermal transport processes. Heat generation, whether due to chemical reactions, exothermic processes or Ohmic heating, significantly influences the thermal behaviour of fluids in engineering applications. It alters the thermal boundary layer,

affecting heat transfer rates and overall system efficiency.

Frequently studied is flowing over the stagnation point, which describes the behaviour of the fluid flow near the region of a surface situated in a stationary or moving body. Recent studies on the stagnation-point flow of hybrid nanofluids with MHD have highlighted their enhanced thermal performance and fluid dynamics, particularly under magnetic field influence and varying nanoparticle concentrations. Numerical analyses, such as in a three-dimensional non-axisymmetric Homann flow of $Al_2O_3/H_2O$ nanofluids, demonstrate improved heat transfer and skin friction with increased magnetic parameters but a decline in performance with higher unsteadiness, alongside stability validation of dual solutions [24]. The study of MHD stagnation-point flow of hybrid nanofluids, particularly alumina-graphene/water, explores the influence of magnetic and wall permeability parameters on buoyancy-driven dual similarity solutions over a permeable plate [25]. Findings highlight that these parameters extend the solution range and reduce boundary layer thicknesses, with assisting flow yielding higher skin friction and Nusselt numbers compared to opposing flow regimes. Khashi'ie et al. [26] studied MHD unsteady separated stagnation-point flow and revealed that dual solutions occur in decelerating flow, with critical parameters like the Hartmann number, and acceleration significantly influences boundary layer behaviour and thermal performance. Zainodin et al. [27] investigated the stagnation-point flow of hybrid ferrofluids in the presence of MHD, incorporating magnetite and cobalt ferrite nanoparticles in water, highlighting the effects of magnetic fields, viscous dissipation, Joule heating and convective boundary conditions. Key findings include dual solutions under opposing and assisting flows, enhanced skin friction with nanoparticle addition, reduced heat transfer rates due to magnetic fields and viscous effects, and significant thermal rate improvement with higher Biot numbers.

Following the brief literature review, a potential gap was discovered in studying the problem of MHD unsteady separated stagnation-point flow and the thermal progress of $Fe_3O_4$ – $CoFe_2O_4$ over a permeable plate subject to heat generation. This work is an extension of the research of Khashi'ie at al. [8], and in the current study, an optimal solution for different dimensionless parameters has been predicted using statistical tools, namely the response surface methodology (RSM). RSM is a robust statistical technique that has been used to obtain the optimal heat transfer rate [28–30].

## 2. Mathematical model

The modelling of heat transfer in ferrofluid over a permeable moving plate with heat generation has numerous practical applications across engineering, energy systems and biomedical fields. The integration of ferro-nanofluid, which contains magnetic nanoparticles, allows for enhanced control through external magnetic fields. This capability enables specialized applications, including electronic cooling, thermal protection systems, aerodynamic heating management and solar thermal energy optimization.

Hence, this paper covers the unsteady two-dimensional MHD axisymmetric stagnation-point flow and heat transfer of hybrid nanofluid over a permeable moving plate with heat generation illustrated in Fig. 1. The frame of reference $(x, y)$ is chosen in such a way that the $x$-axis is along the direction of the plate and the $y$-axis is normal to the plate. In this problem, the velocity of the plate is defined as $u_0(t) = \partial x_0(t)/\partial t$, where $x_0(t)$ and $t$ are the plate displacement and time, respectively. The free stream velocity, $u_e(t) = \frac{\alpha(x-x_0(t))}{t_{ref}-\beta t} + u_0(t)$, where $t_{ref}$ is the constant reference time, is parallel to the plate. Also, the wall mass transfer velocity is denoted as $v_w(t) = -v_0/\sqrt{t_{ref} - \beta t}$ (where $v_0 < 0$ is the mass suction, and $v_0 > 0$ is the mass injection). In addition, $\alpha$ refers to the strength of free stream velocity outside the boundary layer region. For the unsteadiness parameter, $\beta > 0$ and $\beta < 0$ refer to unsteady accelerating and decelerating parameters, respectively, and $\beta = 0$ denotes a steady boundary layer flow. The permeability of the plate, alongside the unsteadiness of the flow, and the external magnetic field introduce asymmetry in the flow properties (velocity, temperature) across the domain (see [8,31]).

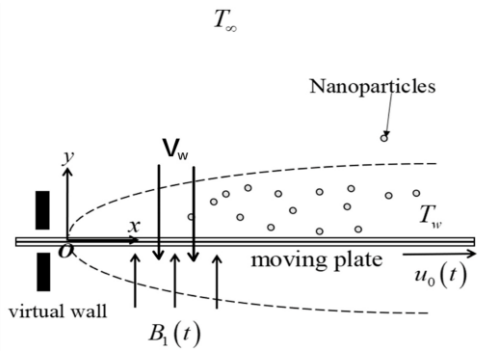


Fig. 1. Geometry of the problem.

The water-based ($H_2O$) hybrid nanofluid incorporates two distinct types of nanoparticles, magnetic-cobalt ferrite ($Fe_3O_4$ – $CoFe_2O_4$). Table 1 presents the properties of thermophysical for each ferroparticle and the based fluid. The mixture of ferroparticles with its based fluid is presumed to be in thermal equilibrium.

Table 1. Thermophysical properties of $H_2O$, $Fe_3O_4$ and $CoFe_2O_4$ [4].

| Thermophysical properties | $H_2O$ (*Bf*) | $Fe_3O_4$ | $CoFe_2O_4$ |
|---|---|---|---|
| $\rho$, kg/m³ | 997.1 | 5180 | 4908 |
| $C_p$, J/(kg K) | 4179 | 670 | 700 |
| $k$, W/(m K) | 0.613 | 9.8 | 3.6 |
| $\sigma$, S/m | $5.5\times10^{-6}$ | $0.74\times10^{6}$ | $1.1\times10^{7}$ |

Using the conservations law, the flow field and energy equations can be modelled as follows:

$$u_x + v_y = 0, \tag{1}$$

$$u_t + uu_x + vu_y = (u_e)_t + u_e(u_e)_x + \frac{\mu_{hnf}}{\rho_{hnf}}u_{yy} +$$

$$-\frac{\sigma_{hnf}}{\rho_{hnf}}B_0^2(u - u_e), \tag{2}$$

$$T_t + uT_x + vT_y = \frac{k_{hnf}}{(\rho C_p)_{hnf}} T_{yy} + \frac{Q_h}{(\rho C_p)_{hnf}} (T - T_\infty), \quad (3)$$

$$u = u_0(t), \quad v = v_w, \quad T = T_w \quad \text{at} \quad y = 0,$$
$$u \longrightarrow u_e, \quad T \longrightarrow T_\infty \quad \text{at} \quad y \longrightarrow \infty. \quad (4)$$

Following Khashi'ie et al. [4], the transformation for Eqs. (1) to (4) is as follows:

$$u = \alpha \frac{x - x_0(t)}{t_{ref} - \beta t} f'(\eta) + u_0(t), \quad v = -\alpha \sqrt{\frac{\nu_f}{t_{ref} - \beta t}} f(\eta),$$
$$\theta(\eta) = \frac{T - T_\infty}{T_w - T_\infty}, \eta = \frac{y}{\sqrt{\nu_f (t_{ref} - \beta t)}}. \quad (5)$$

By using Eq. (5) and after performing the necessary calculation, the following dimensionless momentum and energy equations are attained:

$$\frac{\mu_{hnf}/\mu_f}{\rho_{hnf}/\rho_f} f''' + \alpha(ff'' - f'^2 + 1) - \beta\left(\frac{1}{2}\eta f'' + f' - 1\right) + - \frac{\sigma_{hnf}/\sigma_f}{\rho_{hnf}/\rho_f} M^2 (f' - 1) + 1 = 0, \quad (6)$$

$$\frac{k_{hnf}/k_f}{\Pr (\rho C_p)_{hnf}/(\rho C_p)_f} \theta'' + \alpha f \theta' + - \frac{1}{2}\beta\eta\theta' + \frac{Q_H}{(\rho C_p)_{hnf}/(\rho C_p)_f} \theta = 0, \quad (7)$$

with boundary conditions:

$$f(0) = S, \quad f'(0) = 0, \quad \theta(0) = 1,$$
$$f'(\eta) \to 1, \quad \theta(\eta) \to 0, \quad \text{as} \quad \eta \to \infty, \quad (8)$$

where $M^2 = \sigma_f B_0^2/(\nu\rho)_f$ is the Hartmann number also known as the magnetic field parameter, $\Pr = (\mu C_p)_f/k_f$ is the Prandtl number, $Q_H = Q_h/(\mu C_p)_f$ is the heat generation and $S = -v_0/\alpha\sqrt{\nu_f}$ is the suction parameter. The correlations for the hybrid nanofluid properties are shown in Table 2.

Table 2. Correlations of hybrid nanofluid.

| Properties | Hybrid nanofluid correlation |
|---|---|
| Density | $\rho_{hnf} = \phi_1\rho_1 + \phi_2\rho_2 + (1 - \phi_{hnf})\rho_f$ |
| Dynamic viscosity | $\mu_{hnf} = \frac{\mu_f}{(1-\phi_{hnf})^{2.5}}$, where: $\phi_{hnf} = \phi_1 + \phi_2$ |
| Electrical conductivity | $\sigma_{hnf} = \frac{(\sigma_2 + 2\sigma_{nf} - 2\phi_2(\sigma_{nf} - \sigma_2))k_{nf}}{\sigma_2 + 2\sigma_{nf} + \phi_2(\sigma_{nf} - \sigma_2)}$, where: $\sigma_{nf} = \frac{(\sigma_1(2\phi_1 + 1) + 2\sigma_{Bf}(1 - \phi_1))\sigma_f}{\sigma_f(\phi_1 + 2) + \sigma_1(1 - \phi_1)}$ |
| Heat capacity | $(\rho C_p)_{hnf} = (1 - \phi_{hnf})(\rho C_p)_f + \phi_1(\rho C_p)_{s1} + \phi_2(\rho C_p)_{s2}$ |
| Thermal conductivity | $k_{hnf} = \frac{(k_2 + 2k_{nf} - 2\phi_2(k_{nf} - k_2))k_{nf}}{k_2 + 2k_{nf} + \phi_2(k_{nf} - k_2)}$, where: $k_{nf} = \frac{(k_1 + 2k_f - 2\phi_1(k_f - k_1))k_f}{k_1 + 2k_f + \phi_1(k_f - k_1)}$ |

The local skin friction coefficient and the local Nusselt number are mathematically defined and computed as [25]:

$$\tau_w = \mu_{hnf}(v_x + u_y)_{y=0},$$
$$q_w = -k_{hnf}(T_x + T_y)_{y=0}, \quad (9)$$

where $\tau_w$ and $q_w$ denote the shear stress and the heat flux at a point on the surface of the sheet, respectively. By substituting Eq. (5) into Eq. (9), it yields:

$$\frac{\sqrt{\nu_f (t_{ref} - \beta t)^3}}{\alpha\mu_f (x - x_o(t))} \tau_w = \frac{\mu_{hnf}}{\mu_f} f''(0) \quad (10)$$

$$\frac{\sqrt{\nu_f (t_{ref} - \beta t)}}{k_f (T_w - T_\infty)} q_w = -\frac{k_{hnf}}{k_f} \theta'(0) \quad (11)$$

Here, Eqs. (10) and (11) describe the local skin friction and local Nusselt number, respectively.

## 3. Results and discussion

The solutions of Eqs. (6) and (7), subject to boundary conditions (8), were numerically obtained using the MATLAB's bvp4c solver. Preliminary guesses, optimal boundary layer thickness and various parameter values were carefully selected and adjusted within MATLAB to ensure the most accurate results. The suction effect, S, is considered in this current study. Non-unique or dual solutions for Eqs. (6) and (7) under the conditions of Eq. (8) were found for specific parameter values. The thermal and flow performances of $Fe_3O_4$ – $CoFe_2O_4/H_2O$ were examined and presented in Figs. 2–6, illustrating the variations with the magnetic parameter $M$ = 0, 0.2, 0.4, heat generation parameter $Q$ = 0, 0.1, 0.2, and suction parameter $S$ = 0.1, 0.2, 0.3. Other physical parameters were kept constant throughout the analysis: the Prandtl number Pr = 6.2, volume fractions of the nanoparticles $\phi_1 = \phi_2 = 0.01$, free stream velocity strength $\alpha = 1$.

Figures 2 to 4 illustrate the velocity and temperature profiles under varying values of magnetic field parameters $M$ and heat

generation parameter $Q$ as the governing parameters. All graphical results satisfy the boundary conditions specified in Eq. (8), confirming the validity of the model.

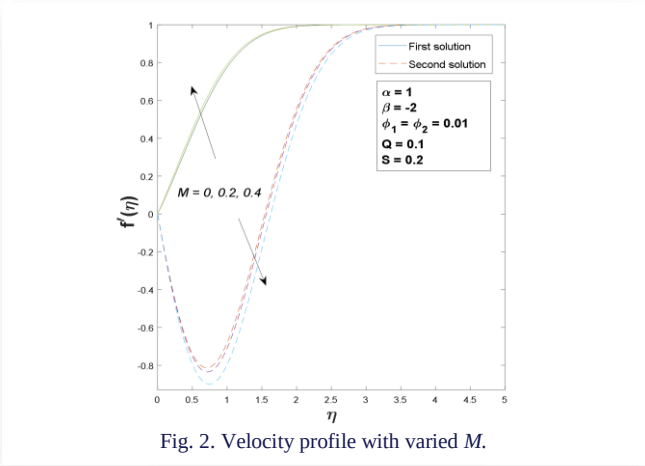


Fig. 2. Velocity profile with varied $M$.

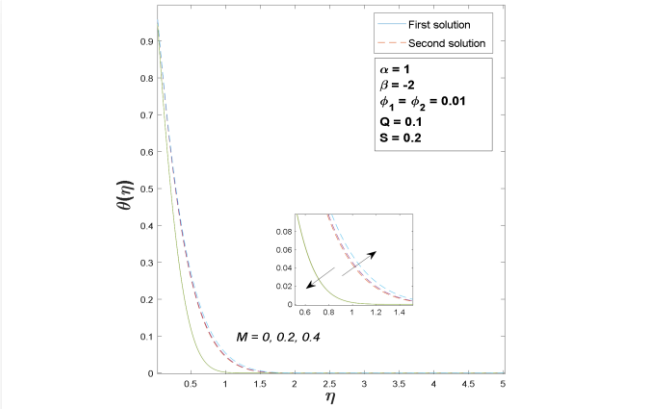


Fig. 3. Temperature profile with varied $M$.

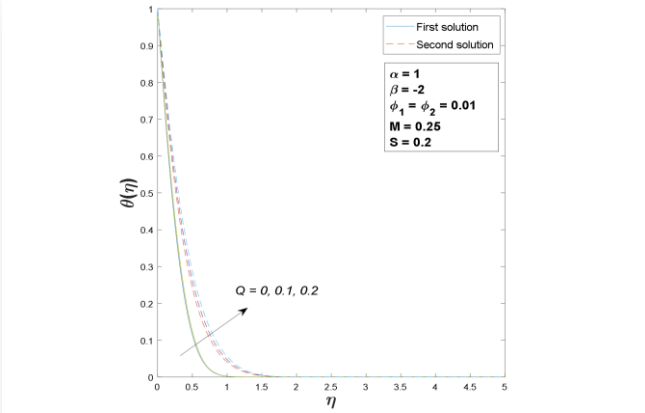


Fig. 4. Temperature profile with varied $Q$.

In Fig. 2, the velocity profile increases with higher $M$, while the temperature profile decreases for the first solution. Both magnetic field and unsteady separated stagnation-point (USSP) flow do not diminish the velocity profile, as the acceleration parameter stabilizes vorticity and facilitates the motion of $Fe_3O_4$ – $CoFe_2O_4/H_2O$. The reduction in the temperature profile seen in Fig. 3 results from the active transfer of heat from the particles into the surrounding cooler surface. The heat generation parameter $Q$ does not influence the flow dynamics; thus, only the temperature profiles are shown in Fig. 4. Both solutions for the temperature profile expand with increasing $Q$, indicating a reduction in the heat transfer rate. This expansion signifies a higher temperature distribution within the fluid, reducing the surface's temperature gradient. Since the heat transfer rate is directly proportional to the temperature gradient, the overall effect is a decreased heat transfer efficiency. This means that the temperature spreads more uniformly across the fluid, reducing the steepness of the temperature gradient near the surface. Since heat transfer depends on this gradient, the overall heat transfer rate reduces, making the system less efficient at dissipating heat.

Figs. 5 and 6 illustrate the profiles of velocity and temperature with varying values of $S$ as the testing factor. Here, the unsteadiness parameter $\beta$ is set at a value $\beta = -2$. All profiles adhere to the boundary conditions in Eq. (8) confirming the model validity. Increasing the suction parameter $S$ causes the velocity profile to increase (approach closer to the boundary) in the first solution, but reduce (move further from the boundary) in the second solution. However, both temperature profiles asymptotically approach the given boundary conditions.

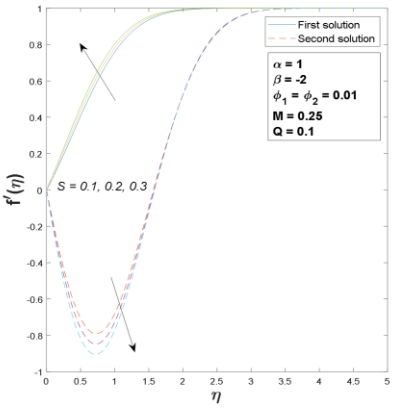


Fig. 5. Velocity profile with varied $S$.

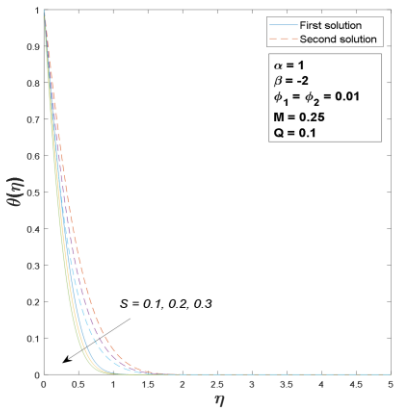


Fig. 6. Temperature profile with varied $S$.

Physically, suction reduces the thickness of the thermal boundary layer by drawing cooler fluid toward the surface, which steepens the temperature gradient at the wall, and enhances the velocity gradient. This process removes the lower-energy, slower-moving fluid from the boundary layer, thereby

thinning it. This leads to improved heat transfer from the surface to the fluid, enhancing the overall heat exchange. Previous studies have highlighted that the heat generation parameter interacts differently with suction. A higher velocity gradient translates into a greater shear stress at the wall, increasing the local skin friction coefficient.

The influence of the suction parameter $S$, on the behaviour of $f''(0)$ and $-\theta'(0)$ with respect to the unsteadiness parameter $\beta_s \le \beta \le 1$ are presented in Fig. 7 and Fig. 8.

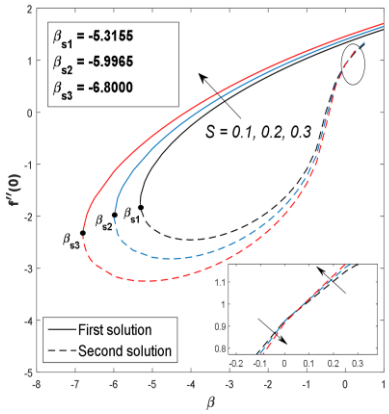


Fig. 7. $f''(0)$ for various $S$.

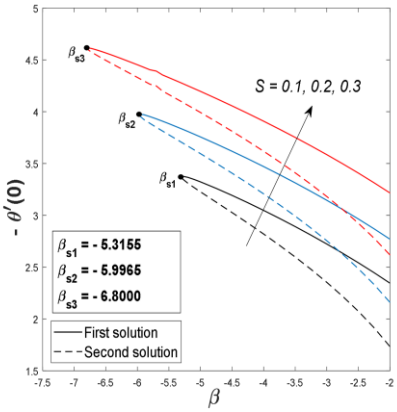


Fig. 8. $-\theta'(0)$ for various $S$.

In stagnation-point flow with heat generation, such as in $Fe_3O_4$–$CoFe_2O_4/H_2O$, suction improves heat removal efficiency, leading to enhanced heat transfer from the surface. Stabilizing the boundary layer and maintaining higher shear stress near the wall, suction helps prevent flow separation. By increasing shear stress near the wall, suction enhances momentum transfer, preventing the detachment of the boundary layer and mitigating flow separation. This stabilization not only improves aerodynamic performance but also enhances convective heat transfer by maintaining a thinner thermal boundary layer. Consequently, suction serves as an effective method for increasing heat transfer efficiency by promoting better energy exchange between the surface and the fluid. Therefore, previous research on dual solutions suggests that the first set of solutions of Eqs. (6) and (7) are stable and physically feasible, while the second set is not.

Multiple solutions are observed for specific values of the governing parameters, extending up to the separation point (critical value of $\beta_s$). It is evident that increasing the suction parameter $S$ expands $\beta_s$. Specifically, $\beta_{s1} = -5.3155$, $\beta_{s2} = -5.9965$ and $\beta_{s3} = -6.8000$ for $S = 0.1, 0.2, 0.3$, respectively. Moreover, the suction parameter increased both $f''(0)$ and $-\theta'(0)$ as $\beta \to +\infty$ but a reduction in $f''(0)$ and an upsurge of $-\theta'(0)$ could be observed for the first solution as $\beta \to \beta_s$.

## 4. Response Surface Methodology

Response Surface Methodology (RSM) is an empirical model that employs the use of statistical techniques to relate input variables to the response. RSM is utilized where the response surface of the heat transfer rate is simulated based on numerical experiments to enhance and optimize the data to determine the optimal values of physical parameters. Some of the widely used experimental designs of RSM compared in terms of its characteristics and efficiency are included, which helps to point out the importance of the design of experiments (DOE) in optimization using RSM. In this study, RSM is applied to determine the optimal conditions and identify which input variables have a significant impact on the heat transfer performance.

In this model, RSM, implemented using Minitab, is utilized to obtain the optimum heat transfer by calculating the local Nusselt number, (response = $\mathrm{Re}_x^{-1/2}\mathrm{Nu}_x = (k_{hnf}/k_f)\theta'(0)$), influenced by three factors: magnetic effect, heat generation, and suction. To perform RSM, the uncoded symbols for these factors were converted into coded symbols, as shown in Table 1. Each parameter is categorized into three levels: low (–1), medium (0), and high (+1), as depicted in Table 3.

Table 3. Varied values of uncoded factors assigned to coded values.

| Uncoded symbol | Coded symbol | Level | | |
|---|---|---|---|---|
| | | Low (–1) | Medium (0) | High (+1) |
| ***M*** | *x*1 | 0.25 | 0.5 | 0.75 |
| ***Q*** | *x*2 | 0.1 | 0.2 | 0.3 |
| ***S*** | *x*3 | 0.1 | 0.2 | 0.3 |

The formula $N = 2^F + 2F + C$ is used to determine the number of runs required, where $F$ represents the number of factors and $C$ represents the number of centre points. To ensure sufficient representation of both factorial and centre points, a total of $N = 20$ trials were conducted, with $F = 3$ and $C = 6$. Table 4 presents 20 runs computed using the involved factors and responses through a face-centred composite design. The following general quadratic regression model is used:

$$\text{response} = \mathrm{Re}_x^{-1/2}\mathrm{Nu}_x = c_o + \sum_{i=1}^{N} c_i x_i + \sum_{i=1}^{N} c_{ii} x_i^2 + \sum_{i=1}^{N-1}\sum_{i=1}^{N} c_{ij} x_i x_j \,, \quad (12)$$

where the response is the dependent parameter or outcome, $c$ represents the coefficient, $N$ is the number of independent variables (factors), and $x$ denotes the factor.

The results are summarized in Table 5 through an analysis of variance (ANOVA). A parameter is considered statistically significant if its p-value is less than 0.05, indicating a 95% confidence level. It can be observed that all variables demonstrated

significance with p-values less than 0.05. As a result, these terms are significant in the correlation of Eq. (12). The final response correlation is then provided as:

$$\begin{aligned}\mathrm{Re}_x^{-1/2}\mathrm{Nu}_x = {} & 2.15690 + 0.02659\,x1 - 1.31010\,x2 + \\ & + 4.04582\,x3 + 0.04281\,x1^2 - 0.2160\,x2^2 + \\ & + 1.1375\,x3^2 + 0.04002\,x1x2 + \\ & - 0.08002x1x3 + 0.75007x2x3. \end{aligned} \quad (13)$$

It can be observed from the coefficients of $x1$ and $x3$ in Eq. (13) that these terms positively affect the response, whereas $x2$ has a negative impact. This implies that the local parameters $M$ and suction parameter $S$ decrease with an increase in $Q$. Physically, this means that removing the slower-moving fluid near the surface enhances heat transfer, and when the fluid itself is generating heat, there is less need for external heat transfer, reducing the efficiency of convective cooling. This observation is consistent with and encapsulates the numerical results presented in the preceding section.

Table 4. Experimental design and response values on $\mathrm{Re}_x^{-1/2}\mathrm{Nu}_x$.

| Runs | Coded values | | | Real values | | | Response |
|---|---|---|---|---|---|---|---|
| | $x1$ | $x2$ | $x3$ | $M$ | $Q$ | $S$ | |
| **1** | -1 | -1 | -1 | 0.25 | 0.1 | 0.1 | 2.45568 |
| **2** | 1 | -1 | -1 | 0.75 | 0.1 | 0.1 | 2.48798 |
| **3** | -1 | 1 | -1 | 0.25 | 0.3 | 0.1 | 2.19294 |
| **4** | 1 | 1 | -1 | 0.75 | 0.3 | 0.1 | 2.23017 |
| **5** | -1 | -1 | 1 | 0.25 | 0.1 | 0.3 | 3.36643 |
| **6** | 1 | -1 | 1 | 0.75 | 0.1 | 0.3 | 3.39166 |
| **7** | -1 | 1 | 1 | 0.25 | 0.3 | 0.3 | 3.13462 |
| **8** | 1 | 1 | 1 | 0.75 | 0.3 | 0.3 | 3.16292 |
| **9** | -1 | 0 | 0 | 0.25 | 0.2 | 0.2 | 2.77836 |
| **10** | 1 | 0 | 0 | 0.75 | 0.2 | 0.2 | 2.80882 |
| **11** | 0 | -1 | 0 | 0.5 | 0.1 | 0.2 | 2.91144 |
| **12** | 0 | 1 | 0 | 0.5 | 0.3 | 0.2 | 2.66607 |
| **13** | 0 | 0 | -1 | 0.5 | 0.2 | 0.1 | 2.34131 |
| **14** | 0 | 0 | 1 | 0.5 | 0.2 | 0.3 | 3.26327 |
| **15** | 0 | 0 | 0 | 0.5 | 0.2 | 0.2 | 2.79091 |
| **16** | 0 | 0 | 0 | 0.5 | 0.2 | 0.2 | 2.79091 |
| **17** | 0 | 0 | 0 | 0.5 | 0.2 | 0.2 | 2.79091 |
| **18** | 0 | 0 | 0 | 0.5 | 0.2 | 0.2 | 2.79091 |
| **19** | 0 | 0 | 0 | 0.5 | 0.2 | 0.2 | 2.79091 |
| **20** | 0 | 0 | 0 | 0.5 | 0.2 | 0.2 | 2.79091 |

Table 5. Analysis of variance (ANOVA) for $\mathrm{Re}_x^{-1/2}\mathrm{Nu}_x$.

| Source | DF | Adj SS | Adj MS | F-value | P-value |
|---|---|---|---|---|---|
| **Model** | 9 | 2.27993 | 0.25333 | 5134957.5 | 0 |
| **Linear** | 3 | 2.27874 | 0.75958 | 15396786.77 | 0 |
| **x1** | 1 | 0.00236 | 0.00236 | 47770.77 | 0 |
| **x2** | 1 | 0.15042 | 0.15042 | 3049066.69 | 0 |
| **x3** | 1 | 2.12596 | 2.12596 | 43093522.85 | 0 |
| **Square** | 3 | 0.00071 | 0.00024 | 4774.17 | 0 |
| **x1*x1** | 1 | 0.00002 | 0.00002 | 399.12 | 0 |
| **x2*x2** | 1 | 0.00001 | 0.00001 | 260.04 | 0 |
| **x3*x3** | 1 | 0.00036 | 0.00036 | 7212.23 | 0 |
| **2-Way Interaction** | 3 | 0.00049 | 0.00016 | 3311.55 | 0 |
| **x1*x2** | 1 | 0.00001 | 0.00001 | 162.35 | 0 |
| **x1*x3** | 1 | 0.00003 | 0.00003 | 648.96 | 0 |
| **x2*x3** | 1 | 0.00045 | 0.00045 | 9123.36 | 0 |
| **Error** | 10 | 0 | 0 | | |
| **Lack-of-Fit** | 5 | 0 | 0 | * | * |
| **Pure Error** | 5 | 0 | 0 | | |
| **Total** | 19 | 2.27993 | | | |

The Nusselt number increases with higher values of magnetic field parameter. Further insights into the interaction effects between independent variables on the response can be obtained using RSM. These interactions are visualized through contour and surface plots, as illustrated in Fig. 9.

In Fig. 9a, the plot suggests a stronger correlation between $Nu_x$ and $x2$ compared to $x1$. As $x2$ increases, there is a noticeable reduction in the response value. While the response value increases with $x1$, the rate of increase appears to be more gradual. Furthermore, there is a more noticeable dependence of the response value on $x3$ than on $x1$. While $x1$ does influence the response value, it appears to be less pronounced than that of $x3$, the higher the value of $x3$, the higher the response value achieved at any $x1$ as shown in Fig. 9b. As presented in Fig. 9c, the response value shows a strong positive correlation with a high value of $x3$. The gradient is steep, meaning that increasing $x3$ causes a significant increase in response value. Hence, the magnetic field $M$ and suction $S$ have a favourable impact on maximizing the heat transfer rate, as the magnetic field interacts with moving fluid particles, enhancing mixing and improving heat dissipation. In contrast, the heat generation parameter $Q$ reduces the local Nusselt number, as an increase in $Q$ leads to a flatter temperature profile, decreasing the surface temperature gradient and consequently lowering both the local Nusselt number and heat transfer efficiency.

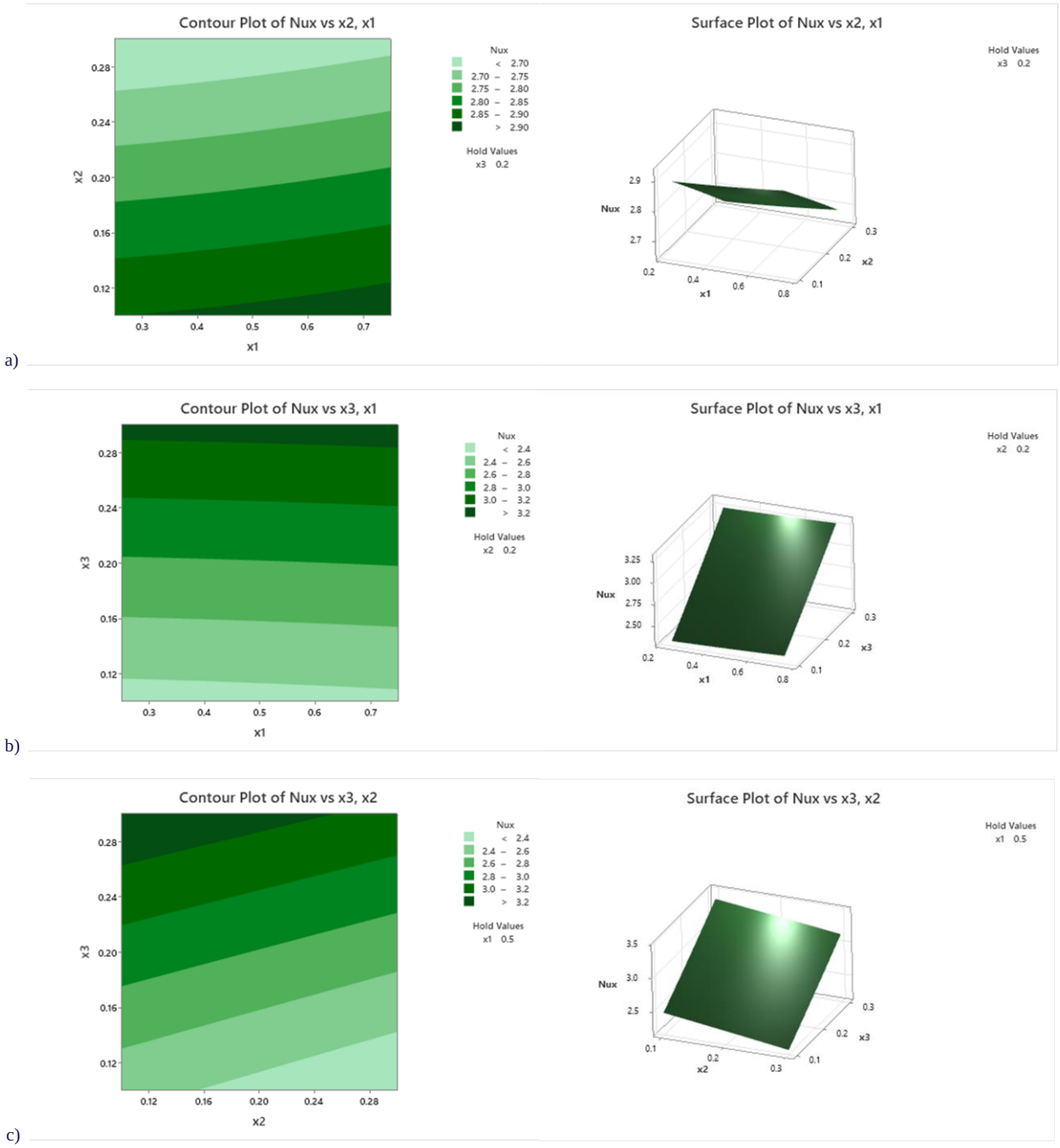


Fig. 9. Contour and surface plots of response (heat transfer) for different combinations of coded parameters.

Finally, the optimization of the local Nusselt number is presented in Table 6. The objective of this optimization is to maximize the local Nusselt number, thereby improving heat transfer performance in the current flow scenario. Achieving desirability of 99.98%, the local Nusselt number reaches an optimized value of 3.39138 when the magnetic effect and suction parameters are at their maximum, while the heat generation parameter is minimized.

Table 6. Optimal value of the response.

| Solution | $x1$ | $x2$ | $x3$ | Response fit | Composite desirability |
|---|---|---|---|---|---|
| 1 | 0.75 | 0.1 | 0.3 | 3.39138 | 0.999769 |

## 5. Conclusions

Thermal progress of unsteady separated stagnation-point flow with the presence of magnetic field, heat generation and suction in hybrid ferrofluid has been successfully analysed. The current investigation used an approach that combined numerical and optimization techniques to examine flow and heat transfer. The similarity transformation technique reduces partial differential equations and boundary conditions into non-linear ordinary differential equations. The dual solution was obtained numerically by utilizing the bvp4c solver in MATLAB. Further, the optimal heat transfer rate was determined by employing the response surface methodology. This study specifically examines the novelty, which is the suction effect. The important discoveries are listed as follows:

- A dual solution was obtained with the first one being the stable and physically feasible.
- Increasing $M$ expands the velocity profile.
- The temperature profile decreases for the first solution, indicating the stabilizing effect of the magnetic field.
- $Q$ primarily affects the temperature profile, with higher values reducing the heat transfer rate.
- An increase in $S$ broadens the range of $f''(0)$ and $-\theta'(0)$, reduces boundary layer thickness, stabilizes the flow, prevents flow separation and increases the skin friction coefficient.
- As the unsteadiness parameter $\beta \to \beta_s$, $-\theta'(0)$ increases for the first solution, demonstrating the effectiveness of suction in optimizing thermal performance.
- The combined effect of suction and magnetic field enhances the heat transfer efficiency, with the suction playing a crucial role in improving heat removal, particularly in stagnation-point flow scenarios.
- The highest heat transfer rates occur at the maximum magnetic field and suction values, while the lowest heat generation results in optimal heat dissipation.

In conclusion, the findings of this study offer significant contributions to the field of fluid dynamics by providing a deeper understanding of fluid flow behaviour and heat transfer mechanisms in hybrid ferrofluids. The research highlights the influence of key parameters, such as the magnetic field, suction and heat generation on thermal performance, which can be beneficial for applications in cooling systems, biomedical engineering and advanced thermal management technologies. Since this study focuses on the flow of hybrid nanofluids containing spherical-shaped nanoparticles, future research could explore the effects of different nanoparticle shapes. Incorporating additional conditions or effects could further extend the applicability of the current flow model to real-world scenarios. As this study is limited to numerical and statistical investigations of thermal behaviour, experimental validation may be considered in future work.

## References


[1] Khan, M., Sarfraz, M., & Zehra, R. (2022). Energy transport near Homann stagnation point flow over a spiraling disk with Cattaneo–Christov theory. *International Journal of Modern Physics B*, 36(25), 2250171. doi: 10.1142/S0217979222501715

[2] Choi, S.U., & Eastman, J.A. (1995). Enhancing Thermal Conductivity of Fluids With Nanoparticles. *ASME International Mechanical Engineering Congress & Exposition*, No. ANL/MSD/CP-84938, CONF-951135-29. November 12–17, San Francisco, USA.

[3] Eastman, J.A., Choi, S.U.S., Li, S., Yu, W., & Thompson, L.J. (2001). Anomalously increased effective thermal conductivities of ethylene glycol-based nanofluids containing copper nanoparticles. *Applied Physics Letters*, 78(6), 718–720. doi: 10.1063/1.1341218

[4] Sarfraz, M, Muhammad, K. Alrihieli, H.F., & Abdelmohimen, M.A.H. (2025). Heat and mass transfer analysis in flow of Walter's B nanofluid: A numerical study of dual solutions. *Journal of Applied Mathematics and Mechanics / Zeitschrift für Angewandte Mathematik und Mechanik*, 105(1), e202300951. doi: 10.1002/zamm.202300951

[5] Anuar, N.S., Bachok, N., & Pop, I. (2021). Influence of MHD hybrid ferrofluid flow on exponentially stretching/shrinking surface with heat source/sink under stagnation point region. *Mathematics*, 9(22), 2932. doi: 10.3390/math9222932

[6] Saranya, S., Al-Mdallal, Q.M., & Javed, S. (2021). Shifted Legendre collocation method for the solution of unsteady viscous-ohmic dissipative hybrid ferrofluid flow over a cylinder. *Nanomaterials*, 11(6), 1512. doi: 10.3390/nano11061512

[7] Waini, I., Khashi'ie, N.S., Kasim, A.R.M., Zainal, N.A., Hamzah, K.B., Arifin, N.M., & Pop, I. (2022). Unsteady magnetohydrodynamics (MHD) flow of hybrid ferrofluid due to a rotating disk. *Mathematics*, 10(10), 1658. doi: 10.3390/math10101658

[8] Khashi'ie, N.S., Waini, I., Zainal, N.A., Hamzah, K.B., Kasim, A.R.M., Arifin, N.M., & Pop, I. (2022). Thermal Progress of Unsteady Separated Stagnation Point Flow with Magnetic Field and Heat Generation in Hybrid Ferrofluid. *Nanomaterials*, 12(18), 3205. doi: 10.3390/nano12183205

[9] Rosli, W.M.H.W., Mohamed, M.K.A., Sarif, N.M., & Ong, H.R. (2023). Convective Boundary Layer Flow of Williamson Hybrid Ferrofluid over a Moving Flat Plate with Viscous Dissipation. *Journal of Advanced Research in Fluid Mechanics and Thermal Sciences*, 112(1), 176–188. doi: 10.37934/arfmts.112.1.176188

[10] Idris, S., Jamaludin, A., Nazar, R., & Pop, I. (2023). Heat transfer characteristics of magnetized hybrid ferrofluid flow over a permeable moving surface with viscous dissipation effect. *Heliyon*, 9(5). doi: 10.1016/j.heliyon.2023.e15907

[11] Zainodin, S., Jamaludin, A., Nazar, R., & Pop, I. (2023). Effects of higher order chemical reaction and slip conditions on mixed

convection hybrid ferrofluid flow in a Darcy porous medium. *Alexandria Engineering Journal*, 68, 111–126. doi: 10.1016/j.aej.2023.01.011

[12] Zainal, N.A., Nazar, R., Naganthran, K., & Pop, I. (2022). Unsteady separated stagnation-point flow past a moving plate with suction effect in hybrid nanofluid. *Mathematics*, 10(11), 1933. doi: 10.3390/math10111933

[13] Khan, A., Jamshed, W., Eid, M.R., Pasha, A.A., Tag El Din, E.S.M., Khalifa, H.A.E.-W., & Alharbi, S.K. (2022). Unsteady electro-hydrodynamic stagnating point flow of hybridized nanofluid via a convectively heated enlarging (dwindling) surface with velocity slippage and heat generation. *Symmetry*, 14(10), 2136. doi: 10.3390/sym14102136

[14] Mahmood, Z., & Khan, U. (2023). Unsteady three-dimensional nodal stagnation point flow of polymer-based ternary-hybrid nanofluid past a stretching surface with suction and heat source. *Science Progress*, 106(1), 00368504231152741. doi: 10.1177/00368504231152741

[15] Khashi'ie, N S., Arifin, N.M., & Pop, I. (2022). Unsteady axisymmetric radiative Cu-$Al_2O_3/H_2O$ flow over a radially stretching/shrinking surface. *Chinese Journal of Physics*, 78, 169–179. doi: 10.1016/j.cjph.2022.06.003

[16] Sarfraz, M., Khan, M, Al Zubaidi, A. & Saleem, S. (2023). Insights into the thermodynamic efficiency of Homann-Agrawal hybrid nanofluid flow. *Alexandria Engineering Journal*, 82, 178–185. doi: 10.1016/j.aej.2023.09.074

[17] Khan, M., Sarfraz, M. Mehmood, S. & Ullah, M.Z. (2022). Irreversibility process analysis for $SiO_2$-$MoS_2$/water-based flow over a rotating and stretching cylinder. Journal of Applied Biomaterials & Functional Materials, 20, 1–15. doi: 10.1177/22808000221120329

[18] Sarfraz, M. & Khan, M, (2024). Energy optimization of water-based hybrid nanomaterials over a wedge-shaped channel. *Scientia Iranica*, 31(1), 71–82. doi: 10.24200/sci.2023.60254.6689

[19] Sarfraz, M., Yasir, M & Khan, M. (2023). Exploring dual solutions and thermal conductivity in hybrid nanofluids: a comparative study of Xue and Hamilton–Crosser models. *Nanoscale Advances*, 50 (23), 6695–6704. doi: 10.1039/D3NA00503H

[20] Wahid, N.S., Arifin, N.M., Khashi'ie, N.S., & Pop, I. (2020). Hybrid nanofluid slip flow over an exponentially stretching/shrinking permeable sheet with heat generation. *Mathematics*, 9(1), 30. doi: 10.3390/math9010030

[21] Eid, M.R., & Nafe, M.A. (2022). Thermal conductivity variation and heat generation effects on magneto-hybrid nanofluid flow in a porous medium with slip condition. *Waves in Random and Complex Media*, 32(3), 1103–1127. doi: 10.1080/17455030.2020.1810365

[22] Bakar, S.A., Wahid, N.S., Arifin, N.M., & Khashi'ie, N.S. (2022). The flow of hybrid nanofluid past a permeable shrinking sheet in a Darcy–Forchheimer porous medium with second-order velocity slip. *Waves in Random and Complex Media*, 1–18. doi: 10.1080/17455030.2021.2020375

[23] Yasir, M., & Khan, M. (2024). Thermal efficiencies of Ohmic cobalt ferrite and magnetite hybrid ferrofluid flow over an exponentially vertically shrinking surface. *Alexandria Engineering Journal*, 90, 120–128. doi: 10.1016/j.aej.2024.01.055

[24] Zainal, N.A., Nazar, R., Naganthran, K., & Pop, I. (2020). Unsteady three-dimensional MHD non-axisymmetric Homann stagnation point flow of a hybrid nanofluid with stability analysis. *Mathematics*, 8(5), 784. doi: 10.3390/math8050784

[25] Pop, I., Rostami, M.N., & Dinarvand, S. (2021). Dual similarity solutions because of mixed convective flow of a double-nanoparticles hybrid nanofluid: critical points and stability analysis. *International Journal of Numerical Methods for Heat & Fluid Flow*, 31(11), 3319–3342. doi: 10.1108/HFF-09-2019-0714

[26] Khashi'ie, N.S., Wahid, N.S., Arifin, N.M., & Pop, I. (2022). Magnetohydrodynamics unsteady separated stagnation-point (USSP) flow of a hybrid nanofluid on a moving plate. *ZAMM-Journal of Applied Mathematics and Mechanics/Zeitschrift für Angewandte Mathematik und Mechanik*, 102(6), e202100410. doi: 10.1002/zamm.202100410

[27] Zainodin, S., Jamaludin, A, Nazar, R & Pop, I., (2023). MHD Mixed Convection Flow of Hybrid Ferrofluid through Stagnation-Point over the Nonlinearly Moving Surface with Convective Boundary Condition, Viscous Dissipation, and Joule Heating Effects, *Symmetry*, 15(4), 878. doi: 10.3390/sym15040878

[28] Algehyne, E.A., Ahammad, N.A., Elnair, M.E., Zidan, M., Alhusayni, Y.Y., El-Bashir, B., & Alzahrani, F. (2023). Entropy optimization and response surface methodology of blood hybrid nanofluid flow through composite stenosis artery with magnetized nanoparticles (Au-Ta) for drug delivery application. *Scientific Reports*, 13(1), 9856. doi: 10.1038/s41598-023-36931-6

[29] Mishra, S., Panda, S., & Baithalu, R. (2024). Enhanced heat transfer rate on the flow of hybrid nanofluid through a rotating vertical cone: a statistical analysis. *Partial Differential Equations in Applied Mathematics*, 11, 100825. doi: 10.1016/j.padiff.2024.100825

[30] Yahaya, R.I., Arifin, N.M, Mustafa, M.S., Pop, I., Ali, F.M., & Isa, S.S.P. M., (2025). Mixed convection hybrid nanofluid flow past a non-isothermal cone and wedge with radiation and convective boundary condition: Heat transfer optimization. *Case Studies in Thermal Engineering*, 66, 105768. doi: 10.1016/j.csite.2025.105768

[31] Dholwy, S. (2016). Magnetohydrodynamic Unsteady Separated Stagnation-Point flow of a viscous Fluid over a Moving Plate. *Journal of Applied Mathematics and Mechanics / Zeitschrift für Angewandte Mathematik und Mechanik*, 96, 707–720. doi: 10.1002/zamm.2014